Balart, J.; Montanes, N.; Fombuena, V.; Boronat, T.; Sanchez-Nacher, L. (2018). Disintegration in compost conditions and water uptake of green composites from poly(lactic acid) and hazelnut shell flour. Journal of Polymers and the Environment. 26(2):701-715. doi:10.1007/s10924-017-0988-3

"Disintegration in compost conditions and water uptake of green composites from poly(lactic acid) and hazelnut shell flour"

J.F. Balart, N. Montanes, V. Fombuena, T. Boronat, L. Sánchez-Nacher

Instituto de Tecnología de Materiales (ITM)

Universitat Politècnica de Valencia (UPV)

Plaza Ferrándiz y Carbonell 1, 03801 Alcoy, Alicante, Spain

Correspondence to: J.F. Balart (jfbalart@dimm.upv.es)

ABSTRACT

Green composites of poly(lactic acid)-PLA and hazelnut shell flour (HSF) with and without epoxidized linseed oil (ELO) as plasticizer/compatibilizer were subjected to different aging conditions such as water uptake by immersion and disintegration in compost soil. The effect of the hydrolytic degradation was analyzed by measuring the weight gain as a function of the immersion time in water and calculating the corresponding diffusion coefficients. As expected, the water diffusion coefficient increases with HSF content while no remarkable change is obtained for plasticized compositions with ELO. Differential scanning calorimetry (DSC) reveals a noticeable increase in crystallinity after the degradation process by water immersion. Degradation in controlled compost soil was followed thorough measurements of weight changes. In general, the weight change for a particular degradation time is lower as the HSF content increases. In addition, presence of ELO as plasticizer/compatibilizer delays the degradation process in compost soil. Scanning electron microscopy (SEM) highlighted a noticeable deterioration of aged samples after two weeks with multiple crack formation and high surface abrasion due to microbial activity after four weeks.

Keywords: poly(lactic acid), PLA; hazelnut shell flour; water uptake; disintegration.

1.- INTRODUCTION

Fibers and lignocellulosic particles are widely chosen as reinforcing fillers in the so called "wood plastic composites", WPCs. Today, due to increasing environmental concerns, important research in the field of environmentally friendly plastic composites is being conducted in the field disintegrable polymers (from both petroleum and natural sources) and lignocellulosic fillers obtained as by-products of different industries[1-5]. Natural fibers and particles show important advantages such as their low density, low abrasion, ready availability, renewable source and disintegration in compost conditions. Most of these lignocellulosic materials are by-products of the food and agroforest industry and this leads to highly cost-effective materials. Moreover, their natural origin confers wood like appearance together with high lightness. All these features contribute to a new generation of high environmental efficiency WPCs, characterized by sustainability, no (or very low) waste generation at the end of the life cycle, potential recyclability and/or upgrading, disintegration in compost soil. While conventional WPCs are composed of a petroleum-based commodity plastic, i.e. poly(ethylene)-PE, poly(propylene)-PP, poly(vinyl chloride)-PVC, etc. and lignocellulosic particles from the wood industry, new high environmentally friendly plastic composites include a wider range of biobased and/or disintegrable polymers filled with lignocellulosic materials from different sources to give the so called "natural fiber reinforced plastics" NFRP[6-7]. Use of WPCs and NFRPs as wood substitutes offers a wide range of potential applications, mainly in the building and construction sector in USA and in the automotive industry in Europe[7-12]. Although WPCs offer a wide range of advantages versus wood, mainly related to their cost, easy processing, wood-like appearance, low maintenance, etc. the high hydrophilic nature of the lignocellulosic component makes

them highly sensitive to water uptake and degradation by enzymatic processes and this is an important drawback to overcome. Lignocellulosic particles are characterized by an extremely high hydrophilic nature. Both cellulose and hemicellulose in natural particles present a high number of hydroxyl groups that can easily react/interact with water molecules. This water absorption favours the overall degradation of WPCs and NFRPs as the continuous swelling and drying of particles leads to micro crack formation which has a negative effect on overall mechanical performance of plastic composites[2-3, 11, 13-16].

Among the wide variety of disintegrable polymers in compost conditions, some of them are produced from petroleum sources, i.e. poly(caprolactone)-PCL, poly(butylene succinate)-PBS, poly(butylene adipate-co-terephthalate)-PBAT, etc. while others are derived from renewable sources either directly such as polysaccharides and proteins, derived from renewable sources subjected to chemical processes such as PLA or obtained by bacterial fermentation as it is the case of poly(hydroxyalkanoates)-PHAs. PLA is one of the most widely used biopolymers on an industrial scale. The monomer for PLA is obtained by fermentation of sugar, cellulose and starch rich materials such as potato, corn, wheat, sugarcane, etc.[8, 17-18]. PLA possesses a crystallinity degree of about 37; its glass transition temperature (T_g) is located between 60-65 ^oC and its melting point varies in the 173-178 ^oC range. Concerning its mechanical properties, it is characterized by an elastic modulus in the 2.7 – 16 GPa range. It can be processed in a similar way to polyolefins by conventional processes such as injection moulding, extrusion, blow moulding, etc. Some of the most common applications of PLA cover the biomedical sector, disposable glasses for cold drinks, plastic bags and food packaging, teabags, disposable cutlery, etc.[19-23]. Some recent works have focused on the use of PLA as matrix for green composites with natural fibers such as paddy straw powder, flax fiber, corn starch, coffee grounds, sisal fibers, etc.[24-28]. These thermoplastic

composite materials from renewable resources allow obtaining fully disintegrable green composites characterized by their high environmental efficiency. Several works report the potential of these composites with PLA matrix and natural fibers. PLA-jute and PLA-sisal composites offer high interfacial shear strength by using a previous surface treatment with NaOH and silanes. It has been reported the use of agave, coir, flax, pine, etc. fibers with PLA matrix with excellent mechanical performance without the need of coupling agents[29-33].

On the other hand, it is worthy to note that the polyester structure of PLA makes it highly sensitive to hydrolysis in water or moisture environments. Water molecules can readily react with the ester bonds to give chain fragmentation with the subsequent formation of lactic acid oligomers and other water soluble decomposition products. Luo *et al.* concluded that hydrolysis degradation occurs preferably in the amorphous domains since PLA packed crystallites are more resistant to this degradation[34]. The study by Tham *et al.* confirmed that hydrolytic degradation of PLA leads to a remarkable decrease in the molecular weight. These short chains show increased mobility and this has a positive effect on crystallinity that is usually higher after degradation. During the hydrolytic degradation, lactic acid oligomers (OLAs) favour crystallization of amorphous domains in which, hydrolysis reactions tend to occur[35].

Green composites with PLA matrix also offer an additional feature versus common WPCs since they can fully degrade in controlled compost conditions. Some polymers can degrade in aerobic conditions and anaerobic conditions by soil compost. During aerobic degradation, carbon dioxide and water are the main released products while anaerobic degradation leads to formation of methane and water[36-38]. Specifically, the mineralization processes during microbial degradation of PLA are developed by microorganisms such as *Fusarium moniliforme, Penicillium roquefort, Amycolatopsis, Bacillus brevis o Rhizopus delemer*[21, 23, 28, 39-40]. According to

Karamanlioglu *et al.* the degradation process of PLA involves two stages in which a chemical hydrolysis reaction (first stage) in the presence of water is followed by microbial degradation (second stage). Lactic acid oligomers (OLAs) are mineralized by some microorganisms to release carbon dioxide (in aerobic conditions) and/or methane (in anaerobic conditions)[37]. Ray *et al.* concluded that the disintegration of PLA is such a complex phenomenon that starts with water absorption and the subsequent breakage of ester bonds leading to oligomer formation[41]. After this, oligomer solubilisation occurs and these oligomers are metabolized by certain microorganisms. Low molecular weight PLA chains are more sensitive to enzymatic degradation because they present higher concentration of end chain groups[37, 40-46].

In this work biobased thermoplastic composites have been prepared with PLA matrix and HSF with different weight percentages in the 10-40 wt% range. Epoxidized linseed oil (ELO) has been added to provide improved toughness due to its plasticization/compatibilization effects. The intrinsic fragility of neat PLA could be overcome by using plasticizers from renewable resources such as those derived from vegetable oils. Bocqué *et al.* concluded that vegetable oils are appropriate plasticizers for PLA because of two main reasons: on one hand, the fatty acid molecules are intercalated between the PLA polymeric chains and this enables chain mobility. On the other hand, the compatibility between plasticizer molecules and polymer chains thorough ester groups allows somewhat lubricant effect[47]. Recent studies have reported the potential plasticizing effect of plant-derived plasticizers such as epoxidized linseed oil (ELO), epoxidized soybean oil (ESBO), dimer fatty acids, etc[48-54].

The effect of both the HSF and the ELO content on the degradation processes related to water uptake and soil compost is evaluated with the main aim to obtain high environmentally friendly industrial formulations for Wood Plastic Composites.

2.- EXPERIMENTAL.

2.1.- Materials.

PLA Ingeo 6201D was supplied in pellet form by NatureWorks LLC (Minnesota, USA). This commercial grade possesses a melt flow index (MFI) comprised in the 15-30 g/(10 min) measured at 210 ºC. Its density is 1.24 g cm^{-3}. Hazelnut shell wastes (*Corylus avellana*) from the food industry were subjected to a dry milling process in an ultra-centrifugal mill from Retsch GmbH (Hann, Germany). The obtained HSF had an average size below 63 μm and with rounded and homogeneous particles. Epoxidized linseed oil (ELO), CAS number 8016-11-3 was supplied by Traquisa S.L. (Barcelona, Spain). This epoxidized oil is characterized by a molecular weight of 1037 g mol^{-1}, a density of 1.05 g cm^{-3}, a viscosity of 12 p at room temperature and a flashpoint of 287 ºC. Moreover, it is not water soluble. The average lipid profile is: 3-5 % stearic acid, 5-7 % palmitic acid, 14-20 % linoleic acid, 18-26 % oleic acid and 51-56 % linolenic acid.

2.2.- Manufacturing of PLA-HSF composites.

HSF and PLA were dried at 60 ºC for 24 h in an air circulating oven to remove the contained moisture. Table 1 shows a summary of the compositions developed in this work.

Table 1

These formulations were extruded in a twin screw co-rotating extruder from DUPRA S.L. (Alicante, Spain) at a rotating speed of 40 rpm. The temperature profile was set to 176 ºC (hopper), 180 ºC, 185 ºC and 192 ºC (die). After this stage, the compounded materials were pelletized and subsequently molded into standard test samples in an

injection molding machine Meteor 270/75 from Mateu & Solé (Barcelona, Spain) at an injection temperature of 190 ºC.

2.3.- Water uptake of PLA-HSF composites by water immersion.

The hydrolytic degradation was carried out according the ISO 62:2008 standard with distilled water at 30±1 ºC for an aging period of 130 days. The sample size was 80x10x4 mm^3 and before the water immersion, samples were dried at 60 ºC for 24 h to remove residual moisture in an air circulating oven mod. 2001245 Digiheat-TFT from J.P. Selecta S.A. (Barcelona, Spain). Samples were taken out the immersion bath every planned period and dried with secant paper and subsequently weighed in an analytic balance mod. AG245 from Mettler Toledo Inc. (Schwerzenbach, Switzerland) and then, immersed in the water bath again. All tests were carried out in triplicate to ensure reliability. Average values of the weight gain were calculated as well as the statistical errors. The total absorbed water, Δm_t, during the immersion was calculated by the following equation.

$$\Delta m_t(\%) = \left(\frac{W_t - W_0}{W_0}\right) \times 100 \qquad \text{Equation 1}$$

Where W_t represents the sample weight after an immersion time t and W_0 is the initial weight of the dry sample before immersion. After a particular immersion time (saturation time) no additional weight gain is observed with increasing time. This saturation weight corresponding to this time is represented by W_s. The ISO 62:2008 allows the application of the Fick's first law to determine the diffusion coefficient, D, from the weight gain data by using Equation 2. The diffusion coefficient, D, can be estimated in the linear region of the weight gain plot. In this zone, $W_t/W_s \leq 0.5$ is a linear

plot of $\Delta m_t = f(\sqrt{t})$ that allows calculation the diffusion coefficient from the slope, θ[13, 35, 55-56].

$$\frac{W_t}{W_S} = \frac{4}{d}\left(\frac{D\,t}{\pi}\right)^{\frac{1}{2}} \qquad \text{Equation 2}$$

Where D is the diffusion coefficient, d is the initial thickness of the sample and W_s is the saturation weight in the linear region. A plot representation of W_t/W_s versus $t^{1/2}$ allows an estimation of the diffusion coefficient by calculating the slope, θ. Then, the diffusion coefficient can be calculated by Equation 3[14].

$$D = 0.0625\,\pi\,d^2\,\theta^2 \qquad \text{Equation 3}$$

Where θ is the slope of the plot of W_t/W_s versus $t^{1/2}$, and d is the initial thickness of the sample. This expression is valid for a one dimensional shape such as a film. The Stefan approximation (Equation 4) considers different corrections to make this expression useful for the three dimensional shapes.

$$D_c = D\left(1 + \frac{d}{h} + \frac{d}{w}\right)^{-2} \qquad \text{Equation 4}$$

Where D_c is the corrected diffusion coefficient which is related to the geometry, h is the total length, w is the width and d is the sample thickness. This equation is based on the assumption that the diffusion rates are the same for all directions[13-15, 55].

2.4.- Disintegration of PLA-HSF composites in controlled compost conditions.

Disintegration test in simulated composting conditions was conducted as indicated by the ISO 20200 standard at a temperature of 58 ºC and a relative humidity of

55 %. Samples sizing 20x20x1 mm^3 were placed in a carrier bag and buried in controlled soil composed (dry weight) of sawdust (40 wt%), rabbit-feed (30 wt%), ripe compost (10 wt%), corn starch (10 wt%), saccharose (5 wt%), cornseed oil (4 wt%) and urea (1 wt%). Samples were periodically unburied from the reactor, washed with distilled water, dried and finally, weighed in an analytic balance. The weight loss due to disintegration in controlled compost soil was calculated by Equation 5. All tests were carried out in triplicate to ensure reliability. Average values of the weight loss were calculated as well as the statistical errors.

$$weight\ loss\ (\%) = \left(\frac{W_0 - W_t}{W_0}\right) \times 100 \qquad \text{Equation 5}$$

Where W_t is the weight of the simple after a bury time t and W_0 is the initial dry weight of the sample.

2.5.- Characterization of aged PLA-HSF composites.

Thermal characterization of the aged samples corresponding to PLA-HSF composites (without and with ELO plasticizer) was carried out by differential scanning calorimetry (DSC) in a DSC mod. 821 calorimeter by Mettler Toledo Inc. (Schwerzenbach, Switzerland). Three different replicates for each formulation were subjected to a dynamic thermal program from 25 ºC to 300 ºC at a heating rate of 10 ºC min^{-1} in nitrogen atmosphere (flow rate of 66 mL min^{-1}). The degree of crystallinity ($\%X_c$) of all materials was calculated by Equation 6.

$$X_{cPLA}\ (\%) = \left[\frac{|\Delta H_m| - |\Delta H_{cc}|}{|\Delta H_{100\%}| \cdot w_{PLA}}\right] \cdot 100 \qquad \text{Equation 6}$$

Where ΔH_m es the melt enthalpy, ΔH_{cc} is the cold crystallization enthalpy, $\Delta H_{100\%}$ is melt enthalpy corresponding to a theoretical 100 % crystalline PLA (-93.7 J g^{-1}) and w_{PLA} is the weight fraction of PLA in the composites[4, 19-20, 57-58].

Surface changes in aged samples were studied by field emission scanning electron microscopy (FESEM) in a Zeiss Ultra 55 from Oxford Instruments (Abingdon, United Kingdom). The acceleration voltage was set to 2 kV and prior to FESEM observation, samples were metallized with a layer of carbon atoms in a high vacuum sputter coater EM MED20 from Leica Microsystem (Milton Keynes United Kingdom).

Colour changes due to ageing were quantitatively assessed by the corresponding colour coordinates in a Hunter spectrophotometer mod. CFLX-DIF-2 by Hunterlab (Murnau, Germany). Colour coordinates in different scales i.e CIE, XYZ, Hunterlab and CIE L*a*b*, were obtained for aged samples and compared to non-aged samples. At least five different measurements were done for each sample and the average values together with the statistical errors were calculated.

3.- RESULTS AND DISCUSSION.

3.1.- Study of the water uptake of PLA-HSF composites.

Fig. 1 shows the evolution of the water uptake as a function of the HSF loading. The weight gain versus the immersion time in water follows typical behaviour as that described by the Fick's law. An initial stage with a rapid weight gain (Δmass) is followed by a second stage with an asymptotic behaviour until saturation or equilibrium ($\Delta mass_\infty$). As expected, the lowest water uptake values are observed for unfilled PLA with a saturation weight of 0.8 wt% after 14 days and remains almost constant until 130 days. Addition of HSF leads to a remarkable increase in the weight saturation values. In addition, a delay in the saturation time is also evident by observing **Fig. 1**. As it can be seen, the saturation time for the PLA composite with 40 wt% HSF is reached for an

immersion time of about 112 days. In addition, the saturation weight increases with the HSF content. The PLA composite with 10 wt% HSF reaches saturation at a weight of 2.2 wt% which is more than twice the value of unfilled PLA while composites with 20 and 30 wt% HSF reach the saturation value at 3.5 and 5.6 wt% respectively. As expected, the maximum water uptake is obtained for the PLA composite with the maximum HSF content in this study (40 wt%) with a saturation weight of 7.6 wt% which represents almost tenfold increase with regard to unfilled PLA. The hydrophilic nature of lignocellulosic particles is responsible for this phenomenon. Cellulose and hemicellulose in HSF contain hydroxyl (-OH) groups that can readily interact with water molecules thus allowing water to enter inside the composite material[5, 13-14, 35, 56, 59]. As the HSF content increases, water uptake occurs in a greater extent until reaching the saturation weight (W_s).

Figure 1

The pronounced hygroscopic nature of the lignocellulosic particles allows water absorption, which leads to particle swelling. This swelling phenomenon contributes to occurrence of internal stresses that finally promote microcrack formation. These cracks also play an important role in the water uptake as they favor water absorption by capillarity processes. **Fig. 2** gathers some FESEM images corresponding to the aged PLA composite surfaces after 130 days immersion time in distilled water. Obviously, the internal stresses associated to particle swelling are more intense for PLA composites with increasing HSF content. For this reason, both the crack occurrence and the crack are more intense for PLA composites with high HSF content. These micro cracks are responsible for a dramatic loss in mechanical properties of composites and even a loss in their structural integrity due to the high embrittlement[3, 5, 13, 16, 56, 60].

Figure 2

Fig. 3 contains the water uptake behaviour of PLA composites with a constant 20 wt% HSF filler content and different epoxidized linseed oil (ELO) content. Our previous results have proved the high efficiency of ELO as plasticizer and compatibilizer in PLA-HSF composites with a remarkable improvement in toughness[61]. In a similar way to that described for PLA composites with varying HSF content, the plot of the weight gain against time indicates a Fickian behaviour. The lowest water uptake is observed for non-plasticized PLA-HSF composite with a saturation weight of 3.5 wt% after 112 days of immersion in water with almost constant value up to 130 days. ELO addition slightly increases the weight saturation values by keeping unvariable the saturation time. In particular, PLA-HSF composites with varying amounts of ELO in the 7.5-22.5 wt% range reach their saturation weight at values of about 4.5 wt% (for all compositions) which is slightly higher than the value for the unplasticized PLA-HSF composite. ELO contributes to slightly more intense water uptake but it seems that the total ELO content does not affect the overall water uptake that it is mainly governed by the HSF content. The epoxidized linseed oil (ELO) provides dual functionality to PLA-HSF composites. On one hand, ELO provides the typical plasticization effect to PLA but on the other hand, it also contributes to improve the polymer-filler interactions by a compatibilization effect. Chieng et al. concluded that only a small amount of plasticizer is placed at the polymer-particle interface in formulations with high plasticizer content[62-65]. The residual plasticizer acts as a typical plasticizer with a remarkable increase in the free volume. The plasticizer molecules are placed between individual polymer chains and, subsequently, intermolecular interactions are weakened thus leading to increased

polymer chain mobility. These phenomena contribute to increase the water uptake[66-68].

Figure 3

Fig. 4 shows FESEM images of the surface appearance of PLA-20 wt% HSF composites with different ELO content after immersion in water. The swollen particles develop strong internal stresses that ultimately, lead to microcrack formation. These microcracks contribute to the water uptake by capillarity processes. It is worthy to note that due to the plasticization effect of ELO, the internal stresses due to particle swelling are less intense than in the unplasticized system. For this reason, PLA-20 wt% HSF composites with the highest ELO content in this study (22.5 wt%) do not show typical crack formation on a fragile matrix. Instead of this, a ductile fracture surrounding the particle can be observed.

Figure 4

The water diffusivity in PLA composites with varying HSF content and PLA-20 wt% HSF with different ELO content can be obtained by the Fick's law. **Table 2** summarizes the diffusion coefficients (D) and the corrected diffusion coefficients (D_c) for all these composites. Regarding the influence of the total amount of HSF in unplasticized formulations it is important to remark a clear increasing tendency in both D and D_c. Neat PLA possesses a corrected diffusion coefficient of 2.31 x 10^{-8} cm^2 s^{-1} which is in total agreement with other values reported in the literature[15, 35, 55-56]. Due to the high hydrophilic nature of the hazelnut shell powder, the only addition of 10 wt% HSF to PLA composites leads to D_c values of 4.03 x 10^{-8} cm^2 s^{-1}. Obviously, as the weight

percentage of HSF increases (e.g. 40 wt% HSF), the diffusion coefficient changes to an eightfold increase with regard to neat PLA[59]. On the other hand, as expected by the water uptake plots in Fig. 3, ELO has only a slight effect on the overall water uptake process. Specifically, the corrected diffusion coefficient changes from 8.67 x 10^{-8} cm^2 s^{-1} for the unplasticized PLA-20 wt% HSF composite up to 8.88 x 10^{-8} cm^2 s^{-1} for the PLA-20 wt% composite containing 22.5 wt% ELO.

Table 2

By means of differential scanning calorimetry (DSC), the main thermal parameters of PLA-HSF composites and PLA-HSF-ELO composites were obtained before the immersion in water and at the end of the aging process (130 days). The glass transition temperature (T_g) seems to be invariable for all PLA-HSF composites thus indicating the HSF load does not affect this thermal parameter. Moreover, the aging time by immersion in water does not affect the T_g value which is located at about 66.5 ^oC for all these PLA-HSF composites[35]. However, addition of ELO leads to a noticeable decrease in the glass transition temperature down to values of 60 ^oC thus giving clear evidence of the plasticization effects that ELO provide to PLA composites. It is also worthy to note that the T_g on plasticized PLA-HSF-ELO composites does not vary with increasing ELO content. This suggests that plasticizer saturation occurs at relatively low plasticizer content as observed in other similar systems[69].

Table 3 gathers some relevant information about thermal parameters of PLA-HSF and PLA-HSF-ELO composites before immersion in water and at the end of the aging process that these composites undergo when immersed in water. Regarding to the effect of HSF content in unplasticized PLA-HSF composites, it is important to remark that the cold crystallization peak temperature (T_{cc}) is lower at the end of the aging

process in water if compared to non-aged samples. Hydrolysis promotes chain scission thus resulting in oligomers that tend to crystallize at lower temperatures. These oligomeric lactic acid (OLAs) chains are more likely to move and form packed structures. For this reason, the required energy for crystallization is lower for fully aged PLA-HSF composites whatever their HSF content[14, 34-35, 56]. On the other hand, the associated cold crystallization enthalpy (ΔH_{cc}) is lower on aged PLA-HSF composites. This could indicate that hydrolysis contributes to lowering both cold crystallization temperature and cold crystallization level.

With regard to PLA-HSF-ELO composites, it is worthy to note that the cold crystallization process disappears for all ELO compositions. Presence of ELO accelerates the hydrolysis processes in long aging hydrolytic conditions. These results are in total agreement with the abovementioned effect of aging on the cold crystallization enthalpy, with a clear decreasing tendency related to the hydrolytic aging. The hydrolytic aging on PLA-HSF-ELO composites is more intense and this leads the cold crystallization process to disappear[34, 55-56]. The melt peak temperature (T_m) does not change in a remarkable way during the aging process although slightly higher values are obtained for all compositions[14, 35, 55].

The degree of crystallinity (X_c) is one of the main parameters to assess the aging process in hydrolytic conditions. Neat PLA is characterized by a degree of crystallinity of 11 % before aging while this is remarkably increased up to 22 % at the end of the aging process. As indicated previously, hydrolysis of PLA chains leads to shorter chains (oligomeric lactic acid fragments) that are more readily arranged into a highly packed structure. Thus the ability to crystallize is higher. On the other hand, the hydrolysis tends to occur in the amorphous areas so that leading to low molecular weight chains that can easily arrange to a packed form[14, 45, 55-56, 60]. With regard to the effect of the total content on HSF, the same tendency can be observed. All aged PLA-HSF composites

show a remarkable increase in the degree of crystallinity at the end of the hydrolytic aging with values 60 % higher to their corresponding non-aged formulations. It is also important to note the nucleating effect that the lignocellulosic particles can provide. Lignocellulosic particles offer a clear nucleating effect which contributes to increased crystallinity levels, even on non-aged materials[4, 18, 20, 61, 70].

Table 3

Regarding the effect of the ELO plasticizer on thermal properties it is important to remark a high increase in crystallinity up to values close to 45 % for PLA-HSF-ELO composites with 15 and 22.5 wt% ELO. As it has been stated, the plasticizer promotes a remarkable increase in the free volume which has a positive effect on chain mobility thus allowing oligomers from lactic acid to arrange in a packed form. As the hydrolytic aging selectively occurs in the amorphous domains, oligomers from lactic acid (OLAs) are formed in these amorphous regions. As they are shorter than non-hydrolysed PLA chains, OLAs are more likely to move. This phenomenon, in conjunction with the remarkable increase in the free volume that ELO plasticizer provides allow oligomers to freely move to a packed structure. Then the amorphous domains are remarkably reduced. It is evident that the opacity or transparency are highly dependent on the amorphous to crystalline ratio. The increased crystallinity derived from the hydrolytic aging process also leads to a whitening process[16, 34, 55]. A simple way to evaluate the aging extent is by measuring the evolution of the colour coordinates. **Table 4** shows summarized values of the colour coordinates (L*a*b*) for PLA-HSF and PLA-HSF-ELO composites before and at the end of the hydrolytic degradation process.

Table 4

The colorimetric study allows obtaining quantitative results regarding the hydrolytic degradation by immersion in water. By following the evolution of different colour coordinates: a*, b* (a* >0 tends to magenta and a* < 0 tends to green; b* >0 tends to yellow y b* < 0 tends to blue) and the luminance L* or clarity (L*=0 corresponds to black and L*= 100 corresponds to white), it is possible to quantitative assess the hydrolytic aging. A whitening corresponds to low a* and b* values in conjunction with high luminance (L*), values (in fact, the L*, a*, b* coordinates for pure white are 100, 0, 0 respectively). The effect of the HSF content on aged PLA-HSF composites is evident with a clear whitening process after hydrolytic aging. The luminance (L*) coordinate increases up to 50 % from the initial value for the PLA-HSF composite containing 10 wt% HSF after 130 days subjected to hydrolytic aging. This effect is even more pronounced as the HSF content in PLA-HSF composites increases by reaching L* values of 50.27 which represents almost twice the value of the non-aged sample. Similar tendency can be observed with regard to the effect of ELO in PLA-HSF-ELO composites. In this case, as hydrolytic degradation occurs in a large extent, the luminance coordinate (L*) reaches values of 61 for the PLA-20 wt% HSF composite with 22.5 wt% ELO.

3.2.- Study of disintegration in controlled compost soil of PLA-HSF composites.

The weight loss during the disintegration process in controlled compost soil of PLA-HSF composites with different HSF loading can be observed in **Fig. 5**. An initial incubation period of about 14 days can be noticed for all compositions including neat PLA. Beyond the incubation period, all composites start the embrittlement process and a quick weight loss. It is important to remark that hydrolytic degradation of PLA is favoured by both temperature and humidity and this test was conducted at a temperature of 58 ^{o}C and 50 % relative humidity. Neat PLA disintegrates faster than PLA

composites with lignocellulosic fillers as reported in literature[24, 40]. After 21 days buried in controlled compost soil, neat PLA has lost about 41 wt% of its initial weight and after a disintegration period of 28 days, the weight loss reaches values of 71 %. Above this time, PLA no longer shows physical consistency and it is fully disintegrated. Addition of lignocellulosic particles leads to a delay in the disintegration rate. As it can be seen in **Fig. 5**, for an elapsed time of 28 days the weight loss is lower than 50 wt% for all PLA-HSF composites regardless their HSF content. This delay is directly related to the fact that PLA-HSF composites possess higher degrees of crystallinity than neat PLA as shown in **Table 3**. The hydrolytic degradation is faster in the amorphous domains, so that, the greater the degree of crystallinity, the greater the resistance to disintegration in compost soil[14, 34, 41, 45, 55]. For an elapsed time of 42 days in controlled compost conditions all PLA-HSF composites show a weight loss of almost 90 %. By observing the degradation rates of all PLA-HSF composites, it is possible to conclude that the HSF content does not affect in a remarkable way to this parameter.

Figure 5

In relation to the effect of the epoxidized linseed oil (ELO) on the disintegration rate of PLA-HSF-ELO composites it is important to remember the two main effects that ELO can provide to PLA-HSF formulations i.e. plasticization and particle-matrix compatibilization[61]. Since ELO addition produces some changes in the internal structure, some changes in the disintegration rate of PLA-20 wt% HSF composites could be produced by ELO as it can be seen in **Fig. 6**.

Figure 6

Disintegration in compost soil starts after an incubation period of 14 days. After an elapsed time of 21 days, unplasticized PLA-20 wt% HSF shows maximum degradation with a weight loss of 19 wt%. Considering the same disintegration period for PLA-HSF-ELO composites with different ELO content, the weight loss is much lower. After 42 days, a maximum weight loss of 86 wt% is detected for the unplasticized PLA-20 wt% HSF composite while all composites with ELO show a weight loss of about 61 wt%. As stablished by the ISO 20200 standard a degree of disintegration of 90 % is needed to consider disintegrable a material. The unplasticized PLA-20 wt% HSF is near this parameter and can be considered disintegrable; nevertheless, addition of epoxidized linseed oil (ELO) changes in a remarkable the degree of integration measured at the same degradation time (42 days). In fact, the total disintegrated weight in composites with different ELO contents is close to 60 wt% which is remarkably lower to the degree of disintegration of the unplasticized PLA-20 wt% HSF with a weight loss near 90 % (86 %) at 42 days. So that, ELO addition leads to a remarkable improvement on polymer-particle interaction but the overall disintegration ability is considerably reduced.

Fig. 7 shows the macroscopic appearance of the samples subjected to the disintegration process in controlled compost soil for PLA-HSF composites with varying HSF content. After an elapsed time of 2 weeks, a clear change in surface topography can be observed. This is representative of the embrittlement process that buried materials undergo in compost. After 4 weeks all samples are disintegrated. As it has been observed previously, addition of HSF delays the disintegration process and after 6 weeks, all samples show no consistency and the test ends.

Figure 7

In the same way, **Fig. 8** gathers some macroscopic pictures of the PLA-HSF-ELO composites subjected to disintegration process in controlled compost conditions. For an elapsed time of 2 weeks, buried samples show a notorious decolouration and the materials are highly embrittled. Whatever the composition in terms of ELO content the disintegration is evident after 4 weeks.

Figure 8

Changes in the surface morphology of the samples along the disintegration in compost soil can be observed in **Fig. 9** and **Fig. 10** which correspond to PLA-HSF and PLA-HSF-ELO composites respectively. Neat PLA, PLA-HSF and PLA-HSF-ELO composites show a very smooth surface before they are buried in compost soil. Samples buried for 2 weeks show many surface cracks which are indicative of the beginning of the degradation process of PLA. The surface crack density is lower for samples containing ELO whatever their content. After 4 weeks, buried samples show a remarkable surface abrasion which leads to more rough and irregular surfaces which correspond to disintegration due to microorganism attack. The diffusion of water from the soil to the composites promotes overall swelling and this phenomenon triggers the microorganism attack with a positive effect on microbial activity[21, 28]. This large surface abrasion is directly related to a high weight loss in the 40 – 50 wt% range for PLA-HSF composites. However, ELO contained in PLA-HSF-ELO composites leads to delayed disintegration and, consequently, the surface abrasion occurs in a less extent while more cracks can be observed as observed in **Fig. 10.**

Figure 9

Figure 10

4.- CONCLUSIONS.

Degradation processes of PLA composites with HSF with and without epoxidized linseed oil (ELO) as plasticizer-compatibilizer in water (water uptake) and in controlled compost soil (disintegration) were studied. By considering the results obtained in the water uptake study, it is possible to evidence the high influence of the HSF content on the overall weight gain. In relation to the effect of the epoxidized linseed oil (ELO) on the water uptake in PLA-HSF-ELO composites, it is worthy to note a slight increase in the water uptake due to increased free volume. On the other hand, the weight percentage of ELO does not affect to the overall weight gain. The weight gains for all PLA-based composites with HSF and ELO follows the Fick's law and a remarkable increase in the diffusion coefficients were observed with increasing HSF loading. Regarding the effect of the epoxidized linseed oil (ELO) plasticizer, only a very slight increase in the diffusion coefficients are observed. The thermal analysis by differential scanning calorimetry (DSC) revealed that the glass transition temperate (T_g) remained almost constant at 66.5 ^{o}C and was not affected by the hydrolytic degradation in water. With regard to the cold crystallization peak temperature (T_{cc}), a remarkable decrease is observed for aged samples in water due to increased chain mobility of the oligomers from lactic acid (OLAs) that are formed during the hydrolytic degradation. Similar tendency was found for the cold crystallization enthalpy (ΔH_{cc}) with decreasing values. One important issue is the remarkable increase in the degree of crystallinity which is remarkably higher in PLA-HSF-ELO composites.

Regarding disintegration in controlled compost soil, the degradation rates for PLA-HSF composites is lower with increasing HSF loading and for an elapsed buried time of 42 days, the disintegration reaches values of 90 %. In a similar way to hydrolytic

degradation in water, addition of ELO leads to a delay in the overall disintegration rate. As per the results, the water uptake hydrolytic process and the disintegration in compost soil indicate that PLA-HSF and PLA-HSF-ELO composites are high efficiency materials for interesting uses as wood plastic composites. They offer a neutral environmental impact as they can fully disintegrate in a reasonable period in controlled compost conditions.

ACKNOWLEDGEMENTS

This research was supported by the Ministry of Economy and Competitiveness - MINECO, Ref: MAT2014-59242-C2-1-R. Authors also thank to "Conselleria d'Educació, Cultura i Esport" - Generalitat Valenciana, Ref: GV/2014/008 for financial support.

REFERENCES

1. Altun Y, Dogan M, Bayramli E (2013) Journal of Polymers and the Environment 21:850-856.
2. Ferrero B, Fombuena V, Fenollar O, Boronat T, Balart R (2015) Polymer Composites 36:1378-1385.
3. Nachtigall SMB, Cerveira GS, Rosa SML (2007) Polymer Testing 26:619-628.
4. Pilla S, Gong S, O'Neill E, Rowell RM, Krzysik AM (2008) Polymer Engineering and Science 48:578-587.
5. Tserki V, Matzinos P, Panayiotou C (2006) Composites Part a-Applied Science and Manufacturing 37:1231-1238.
6. Bogoeva-Gaceva G, Avella M, Malinconico M, Buzarovska A, Grozdanov A, Gentile G, Errico ME (2007) Polymer Composites 28:98-107.
7. Mohanty AK, Misra M, Drzal LT (2002) Journal of Polymers and the Environment 10:19-26.
8. Mukherjee T, Kao N (2011) Journal of Polymers and the Environment 19:714-725.
9. Petchwattana N, Covavisaruch S (2014) Journal of Bionic Engineering 11:630-637.
10. Singh S, Mohanty AK (2007) Composites Science and Technology 67:1753-1763.
11. Summerscales J, Dissanayake N, Virk A, Hall W (2010) Composites Part a-Applied Science and Manufacturing 41:1336-1344.
12. Xie H, Jarvi P, Karesoja M, King A, Kilpelainen I, Argyropoulos DS (2009) Journal of Applied Polymer Science 111:2468-2476.
13. Arbelaiz A, Fernandez B, Ramos JA, Retegi A, Llano-Ponte R, Mondragon I (2005) Composites Science and Technology 65:1582-1592.
14. Gil-Castell O, Badia JD, Kittikorn T, Stromberg E, Martinez-Felipe A, Ek M, Karlsson S, Ribes-Greus A (2014) Polymer Degradation and Stability 108:212-222.
15. Le Duigou A, Bourmaud A, Davies P, Baley C (2014) Ocean Engineering 90:140-148.
16. Porebska R, Rybak A, Kozub B, Sekula R (2015) Polymers for Advanced Technologies 26:1076-1082.
17. Martin O, Averous L (2001) Polymer 42:6209-6219.
18. Perinovic S, Andricic B, Erceg M (2010) Thermochimica Acta 510:97-102.
19. Li S, Wang C, Zhuang X, Hu Y, Chu F (2011) Journal of Polymers and the Environment 19:301-311.
20. Li Y, Venkateshan K, Sun XS (2010) Polymer International 59:1099-1109.
21. Shah AA, Hasan F, Hameed A, Ahmed S (2008) Biotechnology Advances 26:246-265.
22. Yussuf AA, Massoumi I, Hassan A (2010) Journal of Polymers and the Environment 18:422-429.
23. Way C, Wu DY, Cram D, Dean K, Palombo E (2013) Journal of Polymers and the Environment 21:54-70.
24. Kumar R, Yakubu MK, Anandjiwala RD (2010) Express Polymer Letters 4:423-430.
25. Ohkita T, Lee SH (2006) Journal of Applied Polymer Science 100:3009-3017.
26. Wu C-S (2012) Journal of Applied Polymer Science 123:347-355.
27. Wu C-S (2015) Polymer Degradation and Stability 121:51-59.
28. Yaacob ND, Ismail H, Ting SS (2016) Bioresources 11:1255-1269.
29. Birnin-Yauri AU, Ibrahim NA, Zainuddin N, Abdan K, Then YY, Chieng BW (2016) Bioresources 11:3332-3355.
30. Orue A, Jauregi A, Unsuain U, Labidi J, Eceiza A, Arbelaiz A (2016) Composites Part a-Applied Science and Manufacturing 84:186-195.
31. Perez-Fonseca AA, Robledo-Ortiz JR, Gonzalez-Nunez R, Rodrigue D (2016) Journal of Applied Polymer Science 133:9.
32. Regazzi A, Corn S, Ienny P, Benezet JC, Bergeret A (2016) Industrial Crops and Products 84:358-365.

33. Zafar MT, Maiti SN, Ghosh AK (2016) Fibers and Polymers 17:266-274.
34. Luo Y-B, Wang X-L, Wang Y-Z (2012) Polymer Degradation and Stability 97:721-728.
35. Tham WL, Poh BT, Ishak ZAM, Chow WS (2015) Journal of Polymers and the Environment 23:242-250.
36. Itavaara M, Karjomaa S, Selin JF (2002) Chemosphere 46:879-885.
37. Karamanlioglu M, Robson GD (2013) Polymer Degradation and Stability 98:2063-2071.
38. Weng YX, Jin YJ, Meng QY, Wang L, Zhang M, Wang YZ (2013) Polymer Testing 32:918-926.
39. Alimuzzaman S, Gong RH, Akonda M (2014) Polymer Composites 35:2094-2102.
40. Mathew AP, Oksman K, Sain M (2005) Journal of Applied Polymer Science 97:2014-2025.
41. Ray SS, Yamada K, Ogami A, Okamoto M, Ueda K (2002) Macromolecular Rapid Communications 23:943-947.
42. Karlsson S, Albertsson AC (1998) Polymer Engineering and Science 38:1251-1253.
43. Lunt J (1998) Polymer Degradation and Stability 59:145-152.
44. Stloukal P, Pekarova S, Kalendova A, Mattausch H, Laske S, Holzer C, Chitu L, Bodner S, Maier G, Slouf M, Koutny M (2015) Waste Management 42:31-40.
45. Xie L, Xu H, Wang Z-P, Li X-J, Chen J-B, Zhang Z-J, Yin H-M, Zhong G-J, Lei J, Li Z-M (2014) Journal of Polymer Research 21:357.
46. Balakrishnan H, Hassan A, Imran M, Wahit MU (2011) Journal of Polymers and the Environment 19:863-875.
47. Bocque M, Voirin C, Lapinte V, Caillol S, Robin JJ (2016) Journal of Polymer Science Part a-Polymer Chemistry 54:11-33.
48. Darie-Nita RN, Vasile C, Irimia A, Lipsa R, Rapa M (2016) Journal of Applied Polymer Science 133:11.
49. Fernandez SS, Kunchandy S, Ghosh S (2015) Journal of Polymers and the Environment 23:526-533.
50. Ferri JM, Garcia-Garcia D, Sanchez-Nacher L, Fenollar O, Balart R (2016) Carbohydrate Polymers 147:60-68.
51. Jia PY, Zhang M, Hu LH, Zhou YH (2016) Korean Journal of Chemical Engineering 33:1080-1087.
52. Li SH, Xia JL, Xu YZ, Yang XJ, Mao W, Huang K (2016) Carbohydrate Polymers 142:250-258.
53. Tee YB, Talib RA, Abdan K, Chin NL, Basha RK, Yunos KFM (2016) Bioresources 11:1518-1540.
54. Xing C, Matuana LM (2016) Journal of Applied Polymer Science 133:8.
55. Deroine M, Le Duigou A, Corre Y-M, Le Gac P-Y, Davies P, Cesar G, Bruzaud S (2014) Polymer Degradation and Stability 108:319-329.
56. Tham WL, Ishak ZAM, Chow WS (2014) Polymer-Plastics Technology and Engineering 53:472-480.
57. Fischer EW, Sterzel HJ, Wegner G (1973) Kolloid-Zeitschrift and Zeitschrift Fur Polymere 251:980-990.
58. Ke TY, Sun XZ (2001) Journal of Applied Polymer Science 81:3069-3082.
59. Pfister DP, Larock RC (2010) Bioresource Technology 101:6200-6206.
60. Islam MS, Pickering KL, Foreman NJ (2010) Journal of Polymers and the Environment 18:696-704.
61. Balart JF, Fombuena V, Fenollar O, Boronat T, Sanchez-Nacher L (2016) Composites Part B-Engineering 86:168-177.
62. Chieng BW, Ibrahim NA, Then YY, Loo YY (2014) Molecules 19:16024-16038.
63. Chieng BW, Ibrahim NA, Yunus WMZW, Hussein MZ (2013) Journal of Applied Polymer Science 130:4576-4580.
64. Liu H, Zhang J (2011) Journal of Polymer Science Part B-Polymer Physics 49:1051-1083.

65. Silverajah VSG, Ibrahim NA, Yunus WMZW, Abu Hassan H, Woei CB (2012) International Journal of Molecular Sciences 13:5878-5898.
66. Alam J, Alam M, Raja M, Abduljaleel Z, Dass LA (2014) International Journal of Molecular Sciences 15:19924-19937.
67. Burgos N, Martino VP, Jimenez A (2013) Polymer Degradation and Stability 98:651-658.
68. Murariu M, Ferreira ADS, Alexandre M, Dubois P (2008) Polymers for Advanced Technologies 19:636-646.
69. Ferri JM, Samper MD, Garcia-Sanoguera D, Reig MJ, Fenollar O, Balart R (2016) Journal of Materials Science 51:5356-5366.
70. Mathew AP, Oksman K, Sain M (2006) Journal of Applied Polymer Science 101:300-310.

TABLE CAPTIONS

Table 1.- Composition and coding of PLA/HSF composites.

Code	PLA content (wt%)	Hazelnut shell flour content (wt%)	ELO content (wt%)
PLA	100	-	-
PLAHSF10	90	10	-
PLAHSF20	80	20	-
PLAHSF30	70	30	-
PLAHSF40	60	40	-
PLAHSF20ELO7.5	72.5	20	7.5
PLAHSF20ELO15	65	20	15
PLAHSF20ELO22.5	57.5	20	22.5

Table 2.- Values of the diffusion coefficient (D) and the corrected diffusion coefficient (Dc) for PLA-HSF and PLA-HSF-ELO composites.

Code	$D \times 10^{-8}$ ($cm^2\ s^{-1}$)	$D_c \times 10^{-8}$ ($cm^2\ s^{-1}$)
PLA	4.85	2.31
PLAHSF10	8.48	4.03
PLAHSF20	18.21	8.67
PLAHSF30	26.71	12.71
PLAHSF40	41.38	19.68
PLAHSF20ELO7.5	18.24	8.67
PLAHSF20ELO15	18.45	8.77
PLAHSF20ELO22.5	18.68	8.88

Table 3.- Summary of the main thermal parameters, i.e. cold crystallization peak temperature (T_{cc}), cold crystallization enthalpy (ΔH_{cc}), melt peak temperature (T_m), melt enthalpy (ΔH_m) and degree of crystallinity (X_c) for neat PLA, PLA-HSF and PLA-HSF-ELO composites, before and after hydrolytic aging in water.

Code	Tcc (ºC)		ΔHcc (J g^{-1})		Tm (ºC)		ΔHm (J g^{-1})		Xc (%)	
	before	after	before	after	before	after	before	after	before	after
PLA	111.5 ±0.5	101.2 ±0.8	23.67 ±0.22	16.11 ±0.86	170.8 ±0.4	172.1 ±0.9	-33.89 ±0.11	-37.01 ±0.85	11	22
PLAHSF10	104.2 ±0.4	98.6 ±0.9	22.24 ±0.24	15.85 ±0.61	170.8 ±0.4	173.5 ±1.3	-34.19 ±0.21	-35.03 ±1.05	14	23
PLAHSF20	104.8 ±0.5	96.6 ±1.4	20.99 ±0.11	17.23 ±1.06	169.9 ±0.6	173.1 ±0.7	-32.43 ±0.18	-34.78 ±0.92	15	24
PLAHSF30	104.4 ±0.6	98.2 ±0.9	19.09 ±0.23	9.13 ±0.82	169.5 ±0.5	176.0 ±0.9	-31.18 ±0.15	-25.34 ±0.97	18	25
PLAHSF40	103.0 ±0.4	96.9 ±0.7	18.05 ±0.13	9.25 ±0.92	169.1 ±0.5	172.7 ±1.4	-28.07 ±0.13	-23.93 ±1.26	18	26
PLAHSF20ELO7.5	105.3 ±0.4	-	22.84 ±0.19	-	168.8 ±0.3	171.4 ±1.0	-35.85 ±0.17	-26.81 ±0.51	19	39
PLAHSF20ELO15	103.1 ±0.6	-	18.50 ±0.24	-	167.5 ±0.5	169.2 ±0.9	-29.76 ±0.22	-25.92 ±1.01	18	43
PLAHSF20ELO22.5	102.4 ±0.5	-	16.97 ±0.32	-	167.5 ±0.4	170.1 ±1.3	-25.42 ±0.24	-24.39 ±0.62	16	45

Table 4.- Colorimetric coordinates for PLA-HSF and PLA-HSF-ELO composites before and after water immersion (CIE L*a*b* scale).

Code	CIE-L*a*b*					
	L*		a*		b*	
	Before	After	Before	After	Before	After
PLAHSF10	28.27 ±0.20	43.13 ±0.14	7.22 ±0.16	10.33 ±0.03	6.14 ±0.25	14.39 ±0.15
PLAHSF20	28.54 ±0.15	45.79 ±0.13	6.67 ±0.14	10.16 ±0.12	5.90 ±0.16	14.34 ±0.15
PLAHSF30	26.46 ±0.06	47.72 ±0.04	4.98 ±0.32	10.55 ±0.03	3.88 ±0.33	15.25 ±0.08
PLAHSF40	28.99 ±0.19	50.27 ±0.17	6.18 ±0.14	9.82 ±0.09	5.26 ±0.04	14.12 ±0.15
PLAHSF20ELO7.5	24.56 ±0.02	50.54 ±0.31	3.60 ±0.06	8.48 ±0.14	2.87 ±0.11	12.60 ±0.11
PLAHSF20ELO15	24.99 ±0.05	53.11 ±0.05	3.71 ±0.19	8.42 ±0.05	2.84 ±0.13	12.67 ±0.02
PLAHSF20ELO22.5	25.40 ±0.21	61.01 ±0.85	4.04 ±0.16	7.44 ±0.47	3.27 ±0.09	12.21 ±0.72

FIGURE LEGENDS

Figure 1.- Plot of the weight gain versus the immersion time in distilled water at 30 ºC for PLA composites with different weight percentages of HSF.

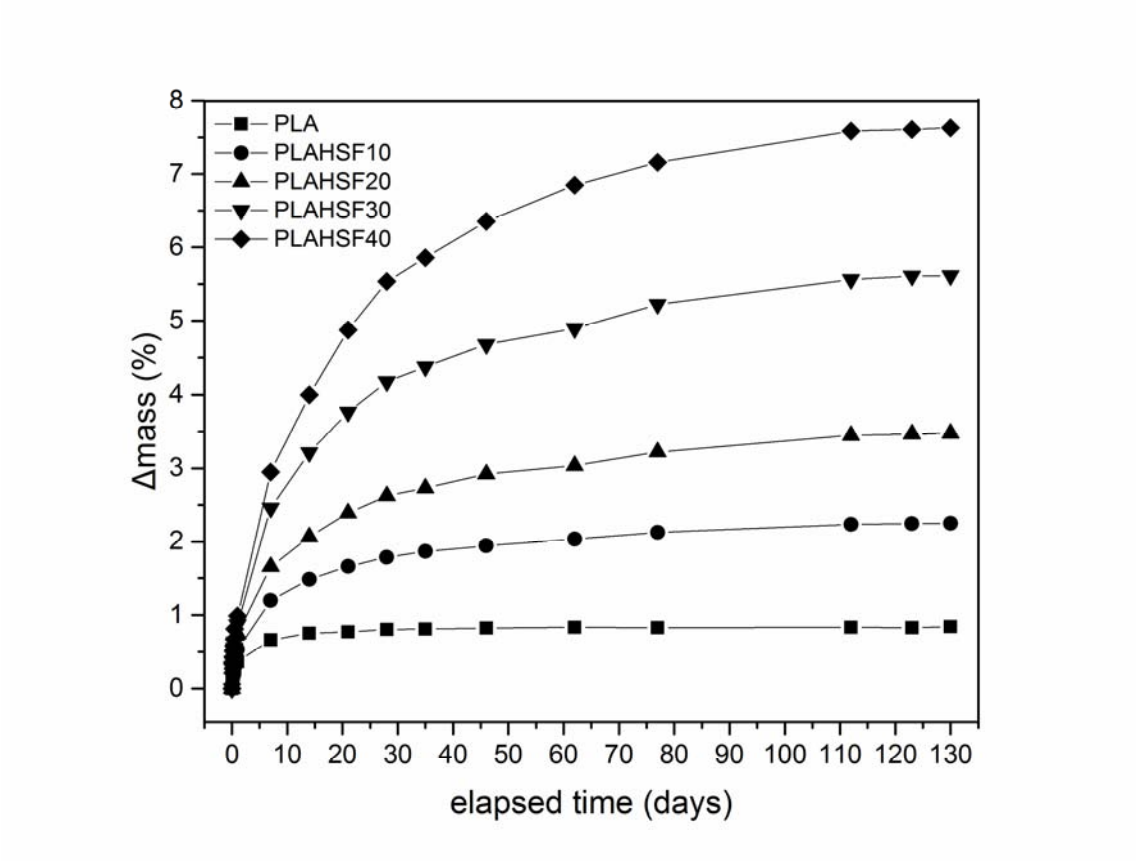

Figure 2.- FESEM images (1000x) of the surface appearance of PLA-HSF composites with different weight percentages of HSF subjected to water uptake for 130 days, a) 0 wt% HSF, b) 10 wt% HSF, c) 20 wt% HSF, d) 30 wt% HSF and e) 40 wt% HSF.

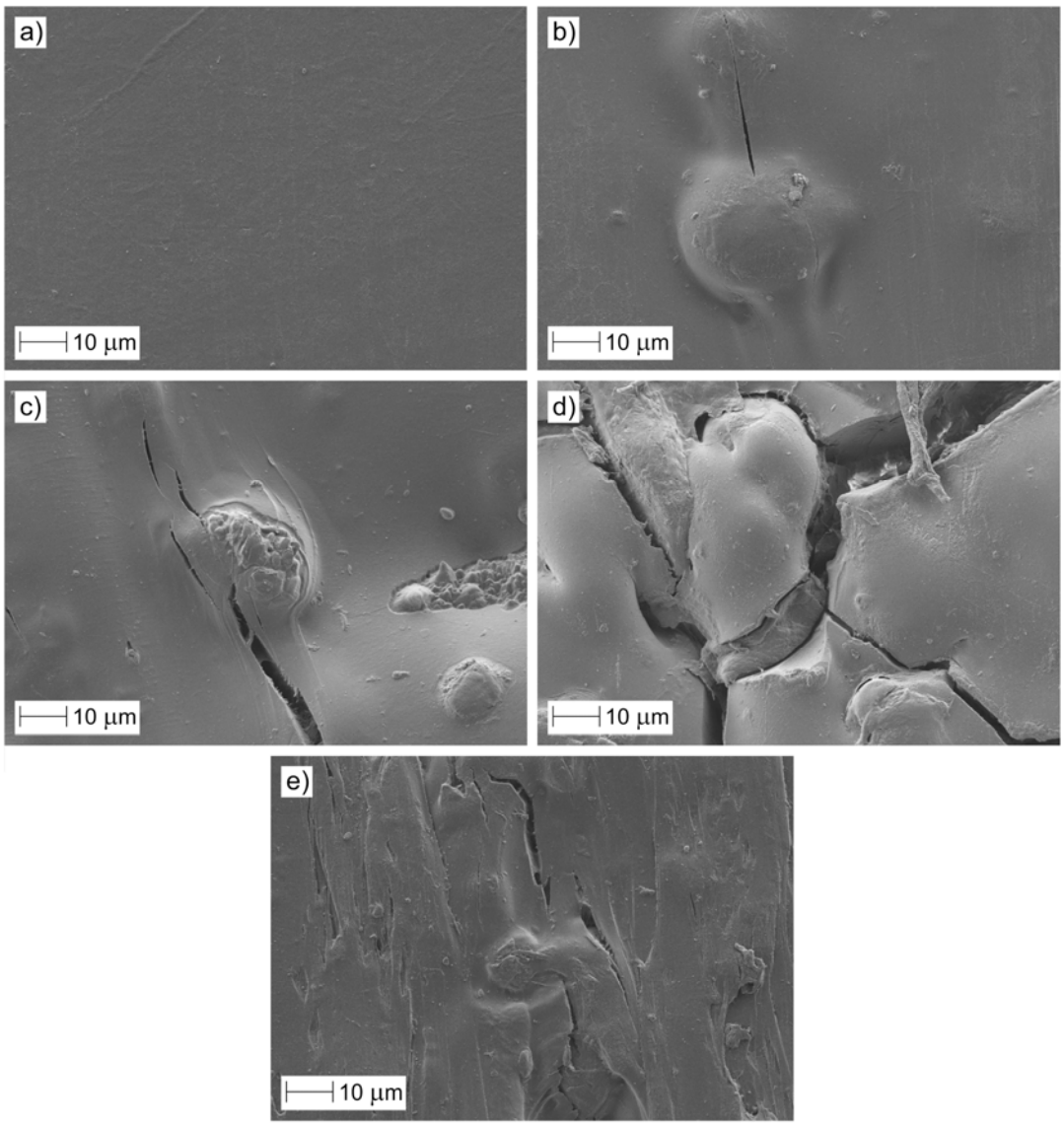

Figure 3.- Plot of the weight gain versus the immersion time in distilled water at 30 ºC for PLA composites with constant HSF content of 20 wt% and different weight percentages of epoxidized linseed oil (ELO).

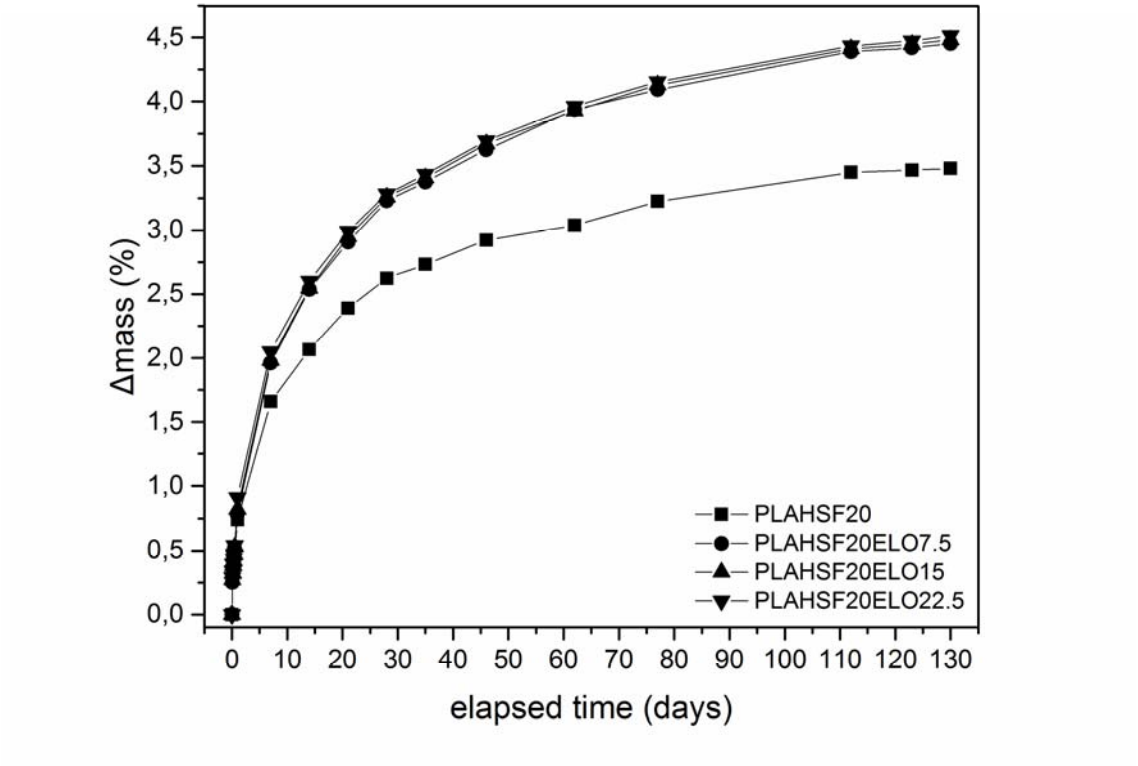

Figure 4.- FESEM images (1000x) of the surface appearance of PLA-HSF-ELO (20 wt% HSF) composites with different weight percentages of epoxidized linseed oil (ELO) subjected to water uptake for 130 days, a) 7.5 wt% ELO, b) 15 wt% ELO and c) 22.5 wt% ELO.

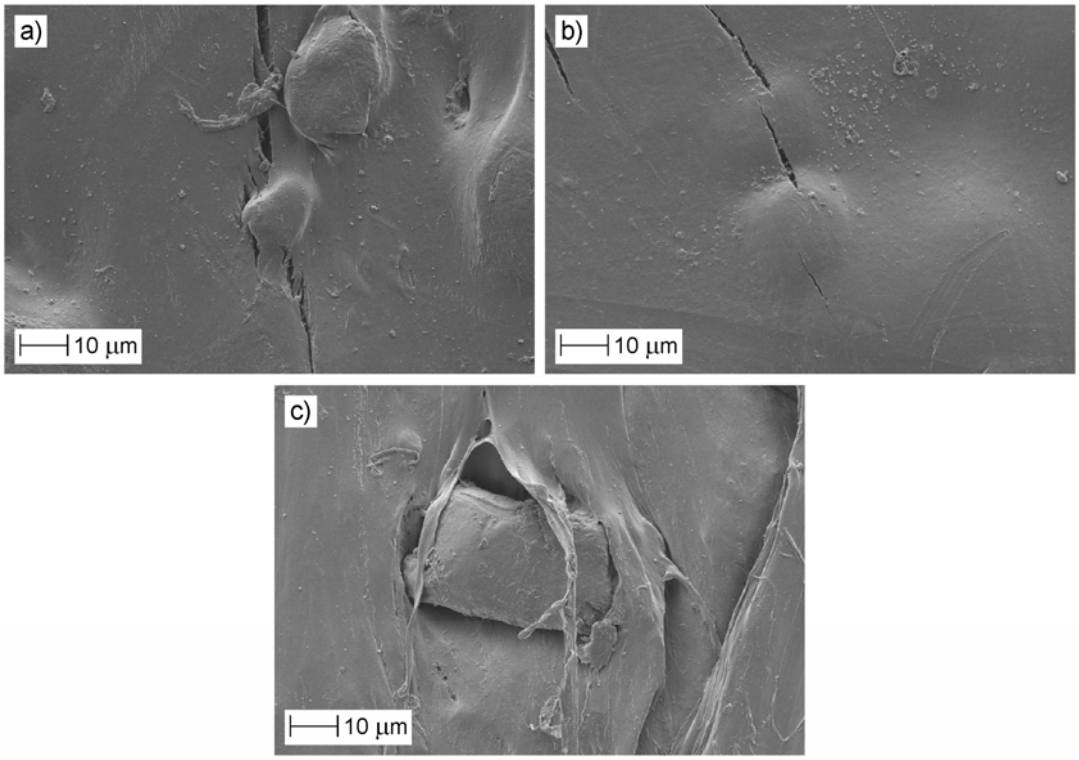

Figure 5.- Percentage weight loss of neat PLA and PLA-HSF composites with different HSF content as a function of the elapsed time during disintegration in controlled compost soil.

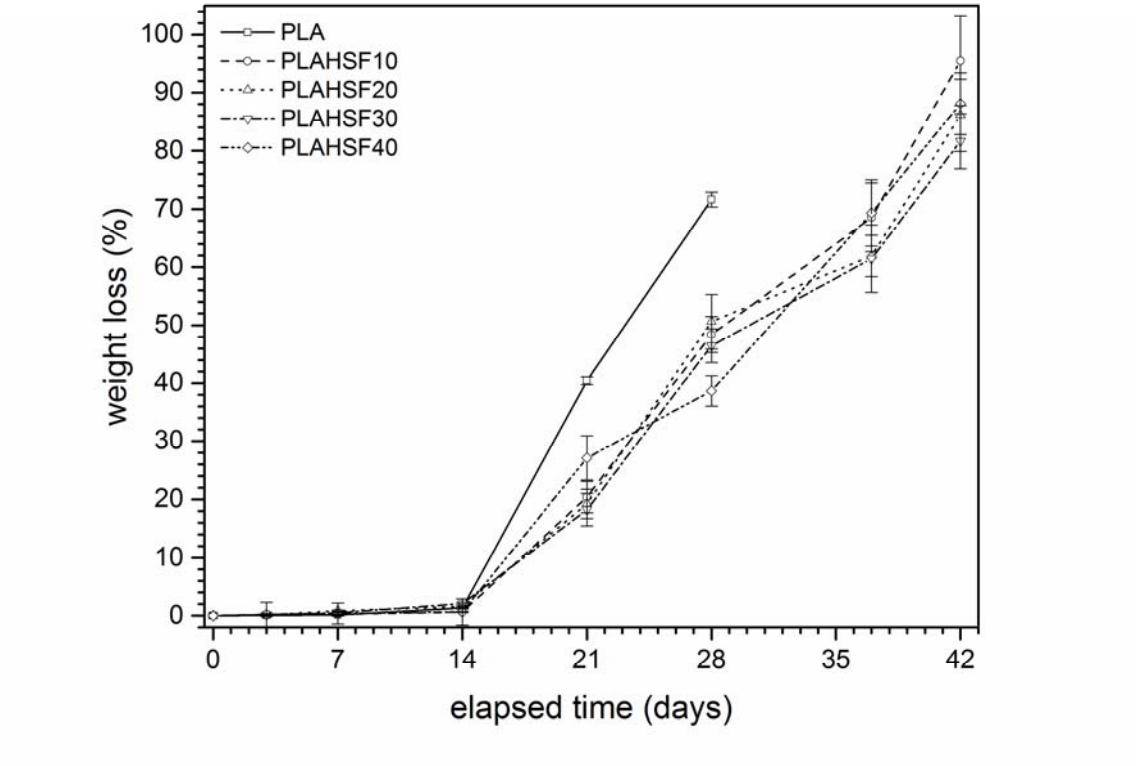

Figure 6.- Percentage weight loss of PLA-HSF-ELO composites with different ELO content as a function of the elapsed time during disintegration in controlled compost soil.

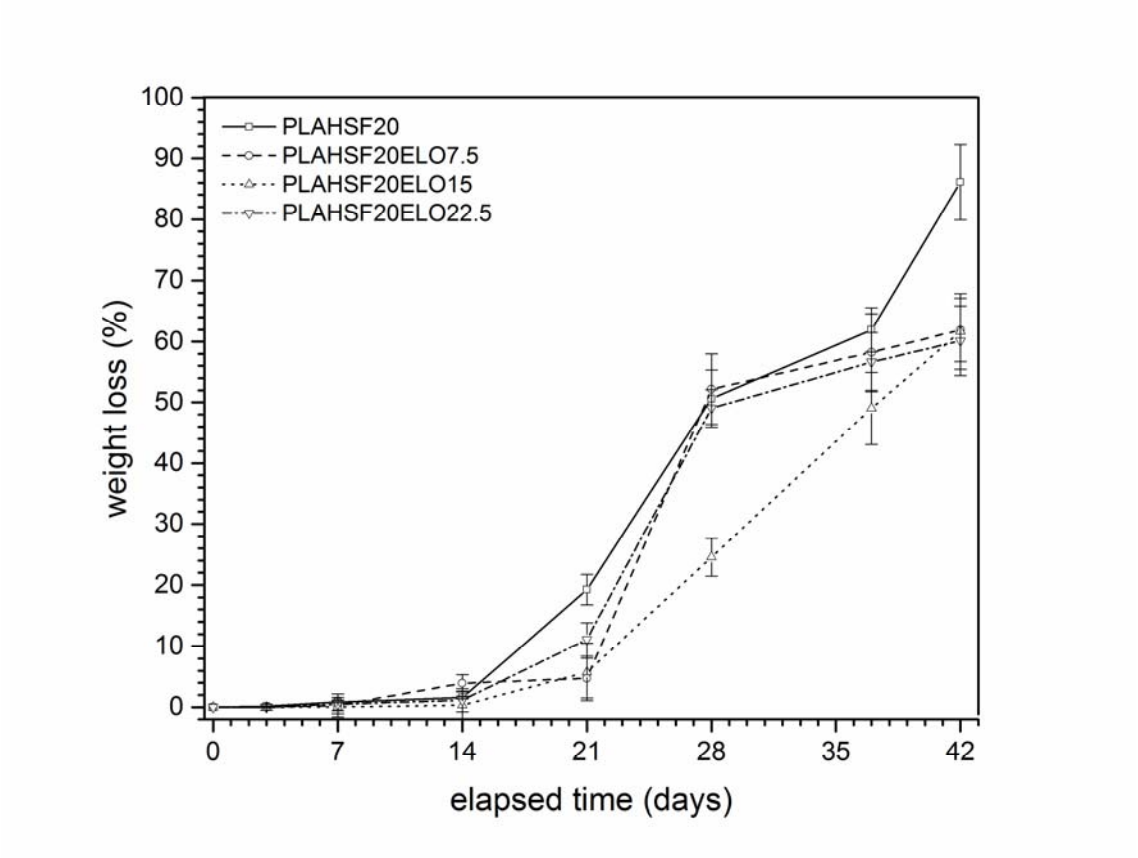

Figure 7.- Macroscopic appearance of PLA-HSF composites during the disintegration test in controlled compost conditions in terms of the HSF content and the elapsed time.

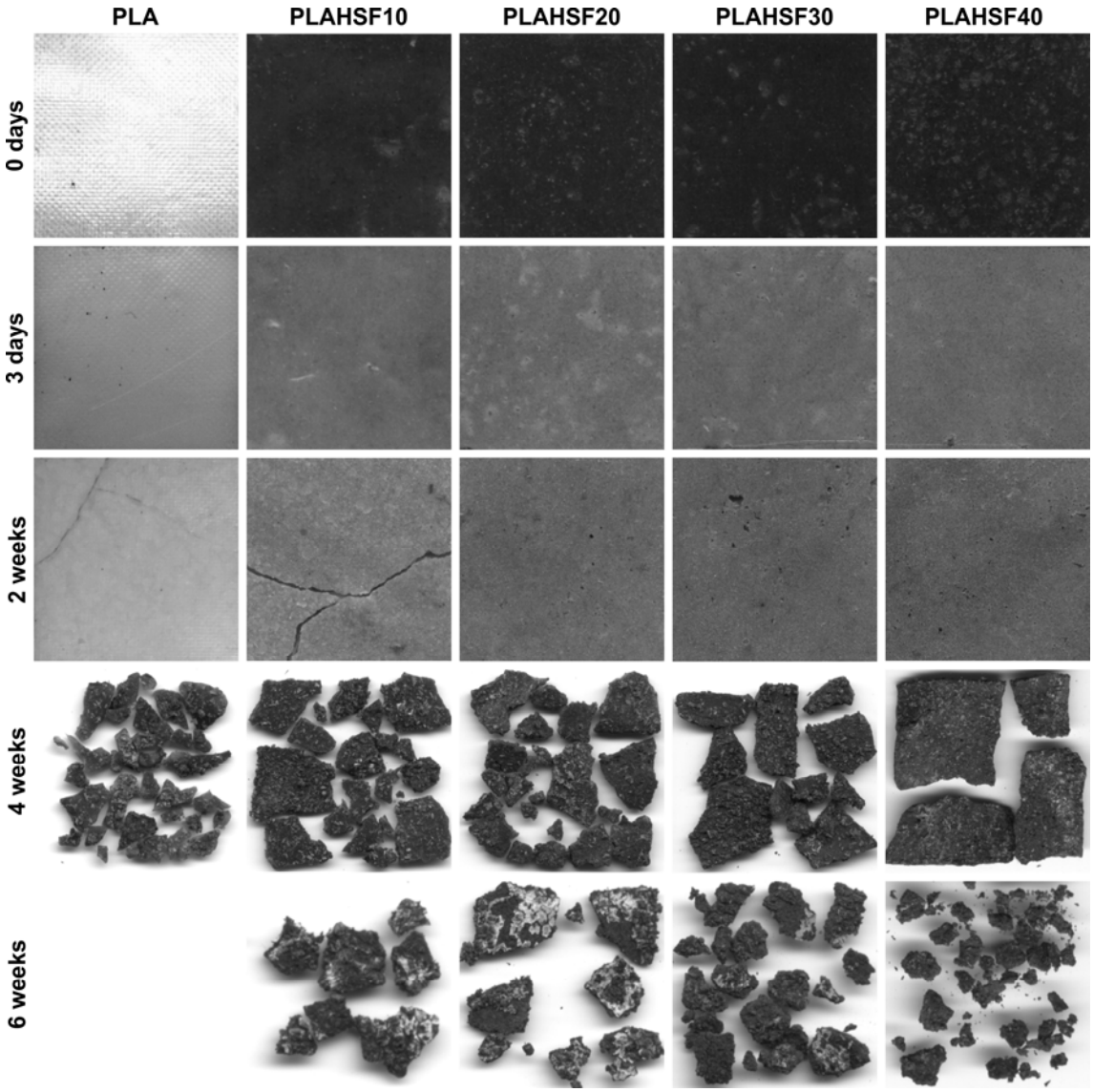

Figure 8.- Macroscopic appearance of PLA-HSF-ELO composites during the disintegration test in controlled compost conditions in terms of the ELO content and the elapsed time.

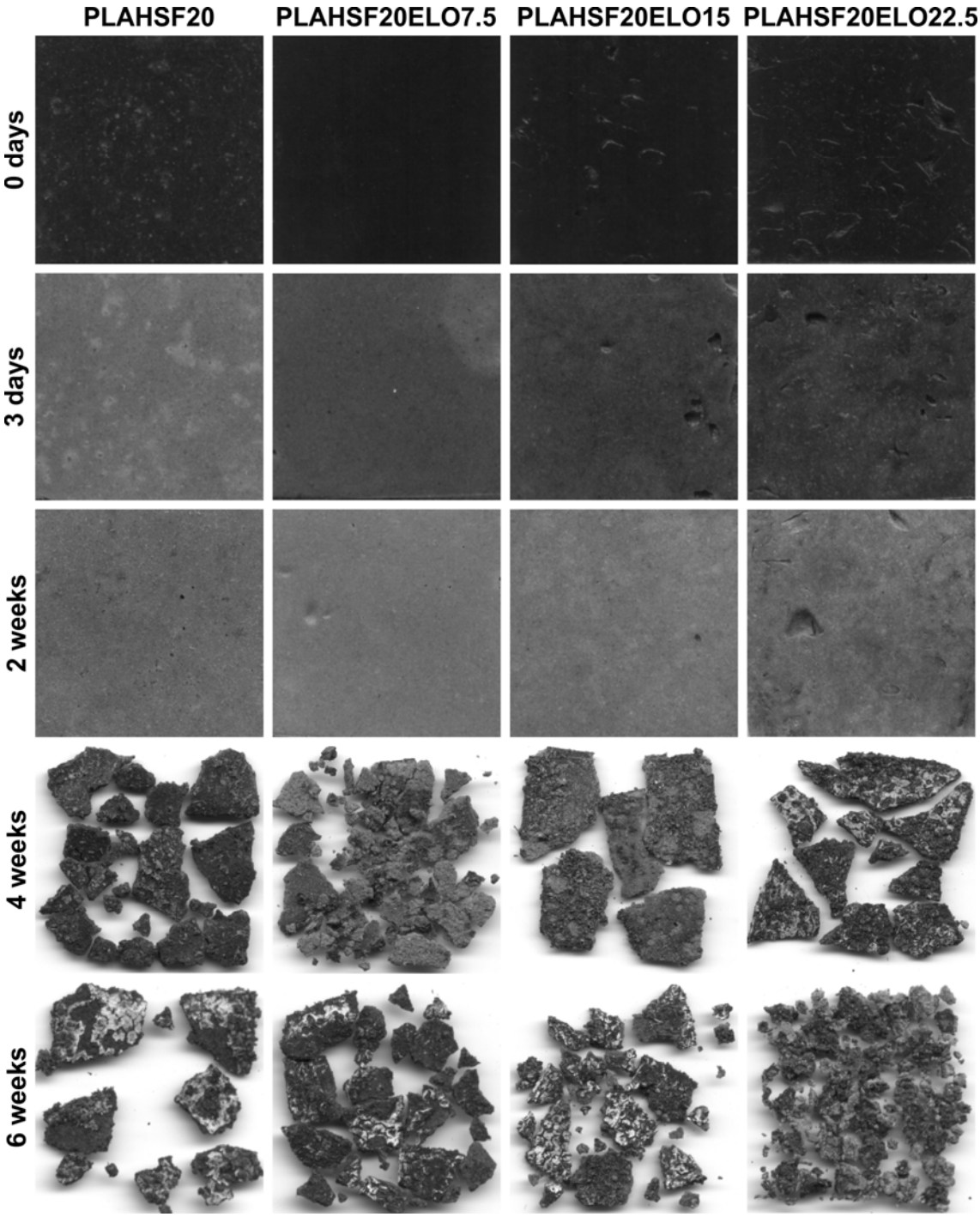

Figure 9.- FESEM images (200x) of the surface appearance of PLA-HSF composites with different weight percentages of HSF subjected to disintegration in controlled compost soil in terms of the elapsed time and the HSF content.

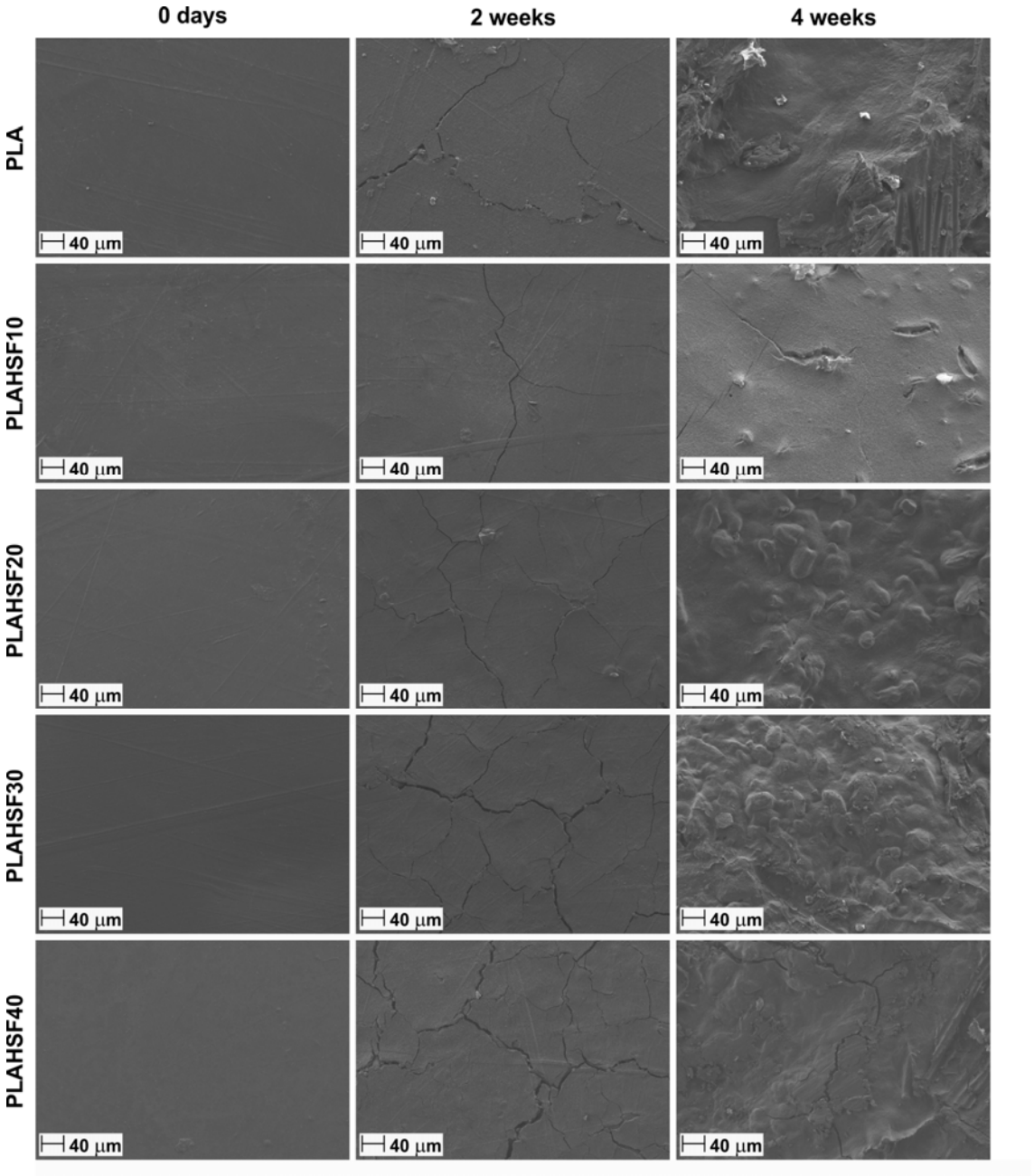

Figure 10.- FESEM images (200x) of the surface appearance of PLA-HSF-ELO composites with different weight percentages of epoxidized linseed oil (ELO) subjected to disintegration in controlled compost soil in terms of the elapsed time and the ELO content.